PAPER

Development of coated heat flux gauges for fast responding measurements

To cite this article: Shawn Siroka *et al* 2022 *Meas. Sci. Technol.* **33** 045104

View the article online for updates and enhancements.

Development of coated heat flux gauges for fast responding measurements

Shawn Siroka[*] ⓘ**, Reid A Berdanier** ⓘ **and Karen A Thole**

The Pennsylvania State University, START Lab, 3127 Research DriveState College, PA, 16801,
United States of America

E-mail: sis5702@psu.edu

CrossMark

Abstract
Thermal systems often exhibit transient behaviors that have important implications for the operation of the system and can be difficult to predict. For these reasons, experimental testing is often required to ensure system durability requirements are achieved. One important parameter governing the survivability of components in hot, high-stress environments is the heat flux into the part that dictates the temperature distribution for the component. However, sensors required to experimentally characterize heat fluxes in extreme environments must also be resilient. This study presents the development of coated heat transfer gauges capable of robust, high-frequency measurements in turbine research facilities. The addition of a protective coating increases the durability of the gauge, but inherent of that coating is the attenuation of high-frequency temperature penetrations. As a result, this study first outlines the use of analytical solutions to define a gauge design for a specific frequency range and heat transfer, ensuring that subsurface signals can be rectified to surface conditions through inverse methods. Then, the fabrication of polyimide substrate sensors with a parylene-F coating is described. Micro surface heaters added to the custom sensors were used to determine important geometric and thermal properties necessary to calculate accurate surface heat flux. Ultimately, this work shows increased sensor robustness in a turbine test bed and experimentally validates that the frequency response of the fabricated sensors meet the design intent.

Keywords: heat flux gauge, coated sensors, high-frequency thermal measurements

(Some figures may appear in colour only in the online journal)

Nomenclature

A	area of gauge
b	RTD half width
c	specific heat
d	thickness
f	frequency $= 0.5\omega\pi^{-1}$
j	imaginary number $= \sqrt{-1}$
k	thermal conductivity
q	heat flux
t	time
T	temperature
X	arbitrary variable
Z	imaginary wave number

Greek

α	thermal diffusivity $= kc^{-1}\rho^{-1}$
ϵ	error in quantity
λ	thermal penetration wave length $\sqrt{2\alpha\omega^{-1}}$
ρ	density
σ	ratio of thermal effusivities
Φ	phase
ω	angular frequency $= 2\pi f$

Subscripts and accents

0	related to the surface condition
1	related to the first temperature device
2	related to the second temperature device

c	related to the coating
cut	cutoff
h	related to surface heating
s	related to substrate
TC	thermocouple
$^-$	mean/DC quantity
$'$	fluctuating/AC quantity
$^\wedge$	amplitude

1. Introduction

Cyclic variations in thermal systems are often difficult to predict. One example of such a system is a gas turbine engine. Because multiple stationary and rotating components with unique airfoil counts operate together within the engine, harmonic mechanical and heat transfer mechanisms (often in excess of 35 kHz [1]) can fatigue hot, highly-stressed turbine blades that operate on a tight thermal margin [2, 3] and, for that reason, accurate time-resolved models are needed. However, such modeling is computationally intensive and often neglects upstream and downstream component interaction, which causes additional undesired harmonic behaviors [2, 4]. Accordingly, extensive experimental testing of the cooling system is paramount to quantify the durability of the actively-cooled turbine blades [4]. To this end, a class of high-frequency measurement devices have been developed and used extensively within the gas turbine community [2].

Although there are many ways to measure heat flux [5], double-sided thin-film resistive temperature detector (RTD) heat flux gauges (HFGs) are uniquely suited for time-resolved temperature and heat flux measurements of turbomachinery components for three reasons: (a) they have a small spatial footprint that is necessary for capturing accurate heat transfer measurements in parts with substantial thermal gradients, (b) their frequency response is on the order of 100 kHz enabling characterization of high-frequency components, and (c) they are minimally intrusive to the flowfield because a flexible substrate is typically used as the sensor base, which allows them to be wrapped around complex airfoil shapes [6]. HFGs are typically composed of two resistive temperature devices deposited on opposing sides of a flexible substrate. The heat flux is calculated by solving the unsteady conduction equation with RTDs providing the temperature boundary conditions and the thermal properties of the substrate defining necessary inputs.

Sensors of this type have been used for decades in turbomachinery applications. Traditionally, HFGs have been used in short-duration facilities with typical test durations on the order of seconds [7–10]. As these sensors transition from short-duration environments to more engine-representative testbeds, additional protections must be deployed to ensure the survivability of the gauges [11]. One such protection is the inclusion of a coating on the surface of the traditional sensor.

The inclusion of a protective coating complicates the fabrication, calibration, and processing of double-sided thin-film RTD HFGs. The coating acts as a thermal damper for high-frequency thermal waves at the surface. Therefore, the coating material and thickness must be chosen such that durability is increased while still capturing the desired flow phenomena. Moreover, attenuated subsurface temperature signals must be rectified to surface conditions through the use of indirect heat conduction problem (IHCP) solutions. Previous work [12] provides guidelines on the design of coated sensors systems capable of utilizing IHCP solutions.

The current study first applies the previous design framework and processing foundation [12] to guide fabrication of coated HFGs specifically designed for use in steady experimental turbine facilities. Then, this work presents calibration procedures with experimental validation of the processing methods. Finally, the durability of the selected coating is validated in the Steady Thermal Aero Research Turbine (START) facility at Penn State University.

2. Design and fabrication of coated sensors

This section serves as a guide to the design and fabrication of coated heat transfer gauges. The steps presented in this section are generalizable to the creation of heat transfer sensors for a variety of high-frequency applications. However, the development of coated heat transfer gauges for specific use in the Penn State START facility will serve as a representative example of the guidelines throughout the entirety of the paper.

The START facility was designed to investigate airfoil heat transfer [13]. This single-stage turbine is capable of engine-relevant operating conditions with true-scale engine hardware. The facility is powered by two 1.1 MW (1500 hp) compressors capable of a providing continuous mass flow to the test section. An in-line 3.5 MW (4700 hp) natural gas heater raises and maintains a main gas path temperature between 395 K to 672 K (250°F to 750°F) while a shell-and-tube heat exchanger cools the secondary air supply to as low as 273 K (32°F). Important to this study, the temperature difference between the main gas path and secondary air sets the magnitude of the heat transfer in the facility for a given aerodynamic condition.

2.1. Gauge design

High frequency heat transfer gauges are required to meet specified criteria critical to the end application. Often, these criteria are linked to the mean heat transfer rate and maximum frequency and magnitude of the time-varying components. One example of a frequency criteria in turbomachinery is the blade passing frequency (BPF), which can drive heat transfer at well-defined regularities. For that reason, the BPF will serve as the minimum frequency response needed for turbomachinery applications.

Table 1 outlines the criteria for the frequency and magnitude used in this particular study. The values in table 1 are typical of turbomachinery applications [10] with exact values determined through the use of computational models at specific testing conditions within the START testbed. Table 1 also details the material choices and thermal properties for the study. The thermal properties for the substrate come from previous tests conducted for the same material [14], while the manufacturer specifications were used for the parylene-F coating properties [15]. These materials and thicknesses were

Table 1. Application criteria and material properties for coated HFG design.

	Parameter	Value	Units
Design criteria	$\widehat{q_0}$	15E3	(W m^{-2})
	$\overline{q_0}$	15E3	(W m^{-2})
	f_{BPF}	8000	(Hz)
	ω_{BPF}	16000π	(rad s^{-1})
Polyimide [14]	$(\rho_s c_s k_s)^{0.5}$	501	(J K^{-1} m^{-2} s$^{-0.5}$)
	k_s	0.19	(W m^{-1} K^{-1})
	d_s	50E-6	(m)
Parylene-F [15]	$(\rho_c c_c k_c)^{0.5}$	407	(J K^{-1} m^{-2} s$^{-0.5}$)
	k_c	0.12	(W m^{-1} K^{-1})
	d_c	1E-6	(m)

Figure 1. Schematic of coated double-sided HFG.

selected for design purposes and will be compared to measured values in subsequent sections.

The selection of polyimide as a substrate and parylene-F as a dielectric coating were constrained foremost by their mechanical flexibility because the application of these sensors requires adhesion around complex airfoils. Additionally, each material must maintain adequate thermal and mechanical properties up to 505 K (450 °F) to meet testing requirements. Furthermore, these materials must be conducive to nanofabrication processes to ensure proper adhesion between layers.

After establishing the end application criteria and material choices, several design parameters are also required: (a) substrate thickness, (b) coating thickness, (c) RTD shape, and (d) RTD material. In practice, the RTD material is constrained by the electro-thermal properties of known materials and is usually nickel [10, 16] or platinum (used for current study) [11, 17, 18]. Moreover, the shape of the RTD for the application of HFGs is constrained in this study by the pursuit of *in-situ* calibration techniques [19], which requires a rectangular shape with large length-to-width ratios ($L/2b = 10$ for current study). Therefore, this section will focus on the thickness choices for the substrate and coating.

Figure 1 shows the general layout of the coated sensor. This design uses platinum thin-film RTDs with copper leads deposited on opposing sides of a flexible polyimide backing and a parylene-F coating deposited on top. Figure 1 also illustrates the thermal properties necessary to deduce the time-resolved surface heat flux (q_0) from the internal temperature measurements (T_1 and T_2).

It is useful to think of these measured (T_1 and T_2) and calculated (q_0 and q_1) quantities in terms of a mean and fluctuating component such that the time-resolved arbitrary variable X is

$$X = \overline{X} + X' \tag{1}$$

where $\overline{X}$ is the mean component and X' is the fluctuating component. The mean heat flux measurements are dependent on the thermal resistance of the substrate layer, but independent of the coating. Consequently, the substrate thickness was chosen based upon the mean heat transfer rate and allowable
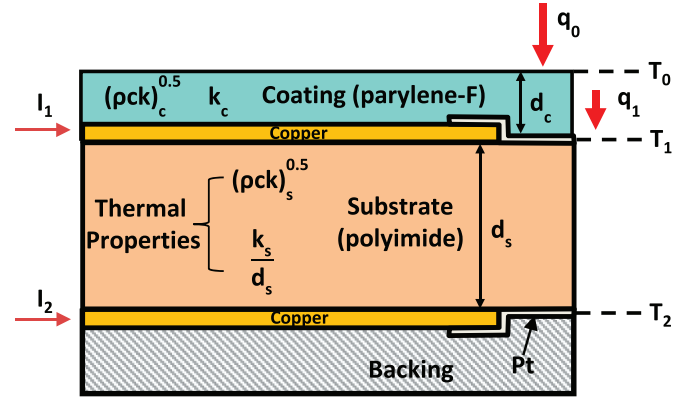
uncertainty in the temperature. This relationship is expressed through equation (2):

$$\overline{q_0} = \frac{k_s \Delta T}{d_s} \tag{2}$$

where k_s is the substrate thermal conductivity, d_s is the substrate thickness, and ΔT is the temperature difference between T_1 and T_2. To minimize uncertainty in mean heat flux, it is advantageous to maximize ΔT across the substrate. As outlined in equation (2), this can be accomplished by increasing the thickness or choosing a substrate material with lower thermal conductivity. Because the thermal conductivity was predetermined in this study based on the substrate material selection, the thermal resistance of the sensor is controlled through the substrate thickness. There exists a trade-off between increasing the measured temperature difference and changing the mean heat transfer in the experiment. Therefore, appropriate care must be taken to ensure the measurement device itself does not affect the thermal results. If the thermal resistance of the sensor gets too large, it will act as an insulation layer causing the experimental setup to deviate from design intent. Particular to this study, a d_s of 50 μms was used which has been previously shown to have negligible effects in similar flow conditions [20].

In addition to considerations of maximizing temperature difference across the substrate, the coating thickness must be chosen to ensure that frequencies of interest are not entirely damped and can be corrected to surface conditions. One available design tool for choosing this parameter is the two-layer analytical solution to the unsteady conduction equation under harmonic heating. The solution to the two-layer harmonic problem outlined by Siroka *et al* [12] develops the relationship between the temperature amplitude at the defined sensor locations ($\widehat{T_1}$ and $\widehat{T_2}$) relative to the surface temperature ($\widehat{T_0}$):

$$\frac{\widehat{T_1}}{\widehat{T_0}} = \frac{2\exp\left(-\frac{d_c}{\lambda_c}\right)}{\sigma + 1 + \exp\left(-\frac{2d_c}{\lambda_c}\right)(1-\sigma)} \tag{3}$$
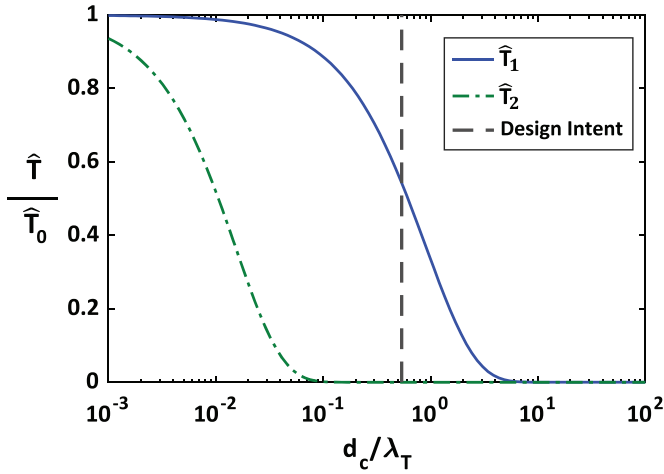
Figure 2. Ratio of surface temperature amplitude to measurement plane temperature amplitudes across a range of non-dimensional coating thicknesses with the selected HFG design intent.
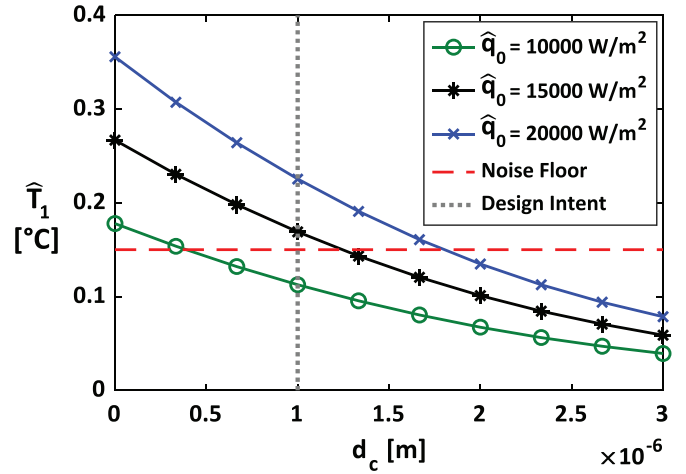

Figure 3. Amplitude of the top temperature sensor at the representative BPF across a range of thicknesses for three different heat flux levels.

and

$$\frac{\widehat{T_2}}{\widehat{T_0}} = \frac{2\exp\left(-\frac{d_c}{\lambda_c}\right)}{\sigma + 1 + \exp\left(-\frac{2d_c}{\lambda_c}\right)(1 - \sigma)}$$
$$*\exp\left[\left(-\frac{d_c}{\lambda_c}\right)\left(\frac{d_s}{d_c}\right)\left(\frac{\alpha_s}{\alpha_c}\right)^{0.5}\right] \quad (4)$$

where the thermal coating wavelength is defined as

$$\lambda_c = \sqrt{\frac{2\alpha_c}{\omega}} \quad (5)$$

and where the ratio of thermal effusivities (σ) is

$$\sigma = \sqrt{\frac{\rho_s c_s k_s}{\rho_c c_c k_c}}. \quad (6)$$

Figure 2 plots these solutions (using values from table 1) and shows the ratio of the measurement-plane temperature amplitudes to surface temperature amplitude across a range of nondimensional coating thicknesses (d_c/λ_c). The nondimensional coating thickness is an important parameter because it represents the factors affecting the attenuation of the measured signal. The design intent plotted in figure 2 is based on the nondimensional coating thickness at a periodic heating frequency, ω_{BPF}, for a coating thickness of 1 μm as outlined in table 1, which will be justified subsequently.

Figure 2 presents several key aspects about the sensor operation. First, at $d_c/\lambda_c = 3$, both $\widehat{T_1}$ and $\widehat{T_2}$ are almost entirely damped relative to the surface temperature fluctuations. This damping represents the loss of information as heat dissipates through the coating and substrate layers. For a given coating thickness value and material, this limit sets the maximum frequency response of the sensor. Second, at design intent ($d_c/\lambda_c \sim 0.5$), the $\widehat{T_2}$ is completely damped from the upstream

layers[1]. Consequently, the gauge at the design intent will operate in a semi-infinite mode [10] meaning the fluctuating heat transfer at the frequency of interest depends only on the temperature measurement at the outward-facing coated surface, $\widehat{T_1}$. Third, at the design intent, the $\widehat{T_1}$ measurement is attenuated from surface conditions due to the coating, by a magnitude of nearly 50%. For this reason, ICHP solutions using inverse methods will be applied to rectify the measured temperature to the true surface temperature [12].

In practice, the coating thickness must be chosen to quantify a specific heat flux level relative to the noise floor of the system. Equations (3) and (4) presents the ratio of measurement to surface temperatures, which is independent of the surface heating value. In contrast, figure 3 shows the temperature amplitude of the top sensor ($\widehat{T_1}$) with a periodic heating at the defined frequency, ω_{BPF}, over a range of coating thickness values for three different heating levels. The formulation of this solution was presented by Siroka *et al* [12] and uses the material properties outlined in table 1. Figure 3 also identifies a representative noise floor (0.15 °C) at the selected BPF for a demonstrative data acquisition system defined here as the combination of HFG signal excitation, filtering, and acquisition. The intersection of the noise floor with the heating curves initially prescribes the limit on the measurable amplitude of instantaneous heat flux for a given coating thickness. However, as will be explored in subsequent sections, signal filtering and averaging can be used to resolve smaller values of heat flux amidst the noise.

2.2. Gauge fabrication

The HFGs used in this study were fabricated at the Penn State University Nanofabrication Laboratory using a custom procedure detailed by Siroka *et al* [11]. The fabrication process

---

[1] It should be noted: to reconstruct the entire frequency spectrum, T_2 is still a necessary input to sufficiently resolve the low frequencies.
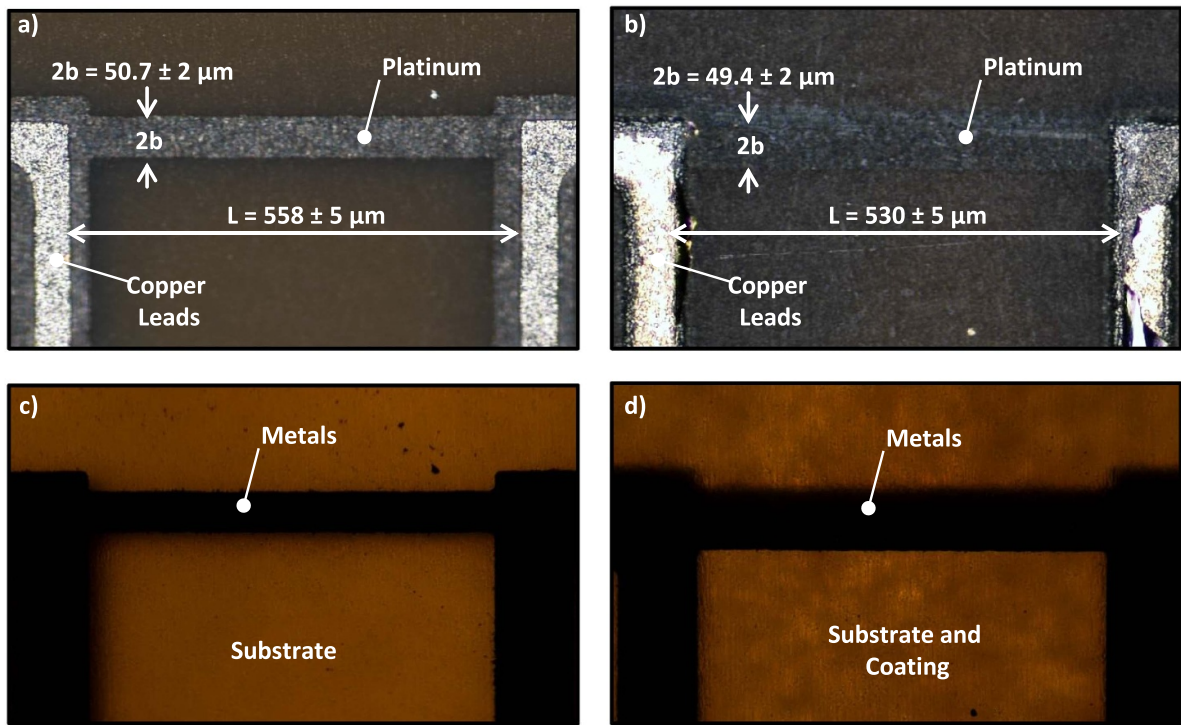
Figure 4. Microscope photos of (a) uncoated HFG and (b) 1 μm parylene-F coated HFG with corresponding geometric measurements under normal illumination; (c), (d) Koehler illuminations of (a), (b), respectively.

involves both additive and subtractive processes starting with a commercially-available Pyralux, which is a 50 μm thick polyimide cladded on both sides with 9 μm of copper. In the first part of the process, copper is removed through an etching process to create the HFG leads. Next, a 1500 Å platinum layer is selectively added through an evaporative deposition process to create the RTD elements. Double-sided sensors can be created by repeating a similar process on the opposite side of the substrate.

The addition of a parylene-F protective coating over the sensors is a new contribution for this study. Parylene-F is inert and chemically resistant, which provides protection against moisture and corrosion [15]. Before applying the coating, an adhesion promotion process was performed using Silane 147 A. The parylene-F was then deposited through a thermal evaporation process that creates a complete-coverage conformal film to encapsulate the copper and platinum layers. Following the deposition, a profilometer was used to quantify the corresponding thickness, which was measured to be 1.00 ± 0.02 μm, illustrating the precise thickness control of the parylene-F coating process.

Figures 4(a) and (b) show the completed uncoated and coated gauges, respectively. It is also noted that figure 4 characterizes two distinct sensor build outcomes, not the same sensor after different processes. These different builds were intended to quantify the durability of the coated sensor to its uncoated counterpart, an effect that will be assessed in more detail in a subsequent section. The design intent for the RTD was a full-width (2*b*) of 50 μm and a length (*L*) of 500 μm. Comparing figures 4(a) and (b), there is a notable decrease

in the platinum-to-polyimide contrast caused by the addition of a coating. To better differentiate platinum from polyimide, a high contrast Koehler illumination is shown in figures 4(c) and (d) corresponding to the standard illumination shown in figures 4(a) and (b). Evaluation of figures 4(c) and (d) shows that the coating did not cause discontinuities within the platinum. Although only a small portion of sensors were used to generate the data for this study, over 200 coated and 200 uncoated sensors were fabricated during this process. No notable differences were present in the yield of the devices.

3. Calibration of coated gauges

To deduce accurate heat flux from the coated gauges, an electrothermal calibration and a material characterization are necessary. The electrothermal calibration transforms the measured voltage across the RTDs to a temperature. These temperatures must then be processed with correct material properties to accurately calculate the thermal energy entering the surface of the HFG. This section outlines the RTD calibration procedure followed by the process used to determine the gauge thermal properties and frequency response for a coated HFG sensor.

3.1. Electrothermal calibration

An accurate and repeatable thermal calibration is necessary for HFGs to operate as intended. To ensure the repeatability of the RTDs, the sensor was annealed under vacuum at
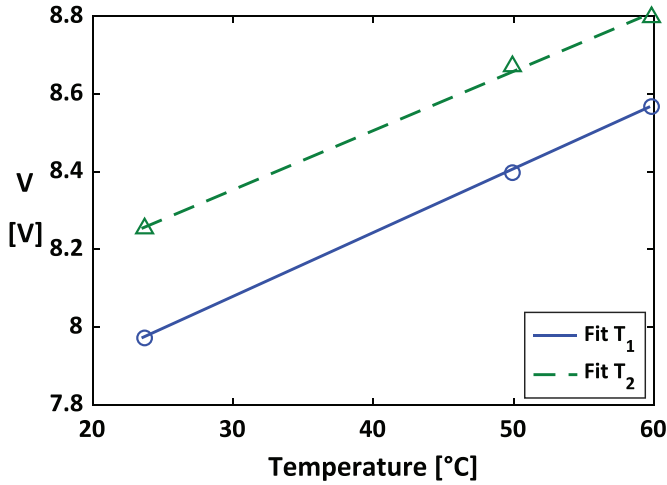
Figure 5. RTD calibration curve for the two sensors comprising the coated HFG.

Figure 6. Schematic of HFG with surface heater used for validation testing.

250 °C after fabrication until the nominal resistance change in the RTDs was less than 0.05% over the span of an hour. This annealing process has been explored in prior studies [19] and has been shown to improve the long-term operation of the devices.

After the annealing process, the coated HFG was placed into a scientific convection oven with a stability rating of 0.2 °C. A precise excitation current of 1.0 mA excites the RTDs as outlined in figure 1, and the measured voltage from the RTD was amplified to improve the signal-to-noise ratio. When thermal equilibrium was achieved, RTD voltages and oven temperature were collected. This procedure was repeated for several temperatures to create the calibration curves shown in figure 5 which are expected to be linear due to the thermo-electric properties of platinum. The calibration curves presented in figure 5 provide a transformation from the measured voltage to the temperature of the RTDs. More information about the annealing and calibration processes can be found in previous works [11, 19].

3.2. Thermal property and frequency response determination

Thermal properties of differential heat flux measurement devices must be properly characterized because they are often the largest contributor to measurement uncertainty. To determine the thermal properties of these particular devices, a heater was deposited on the top of the coating layer, as shown in figure 6. The heater element was fabricated from platinum using the same techniques detailed previously. A small portion of the sensor yield lot were subjected this additional deposition process under the assumption that the material properties of the gauge below the surface heater are representative of the entire build of sensors.

The addition of a surface heater allows for a known heat flux at the surface, which can then be measured using the HFG. Figure 7 illustrates the experimental excitation of this surface heater at room temperature conditions. The heater current, I_0, was set though the use of a custom-designed precision
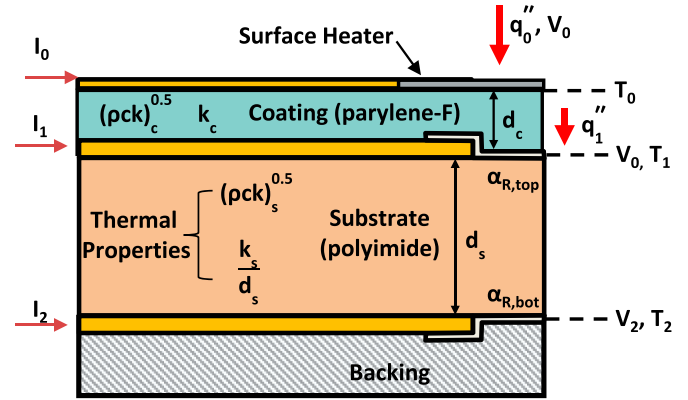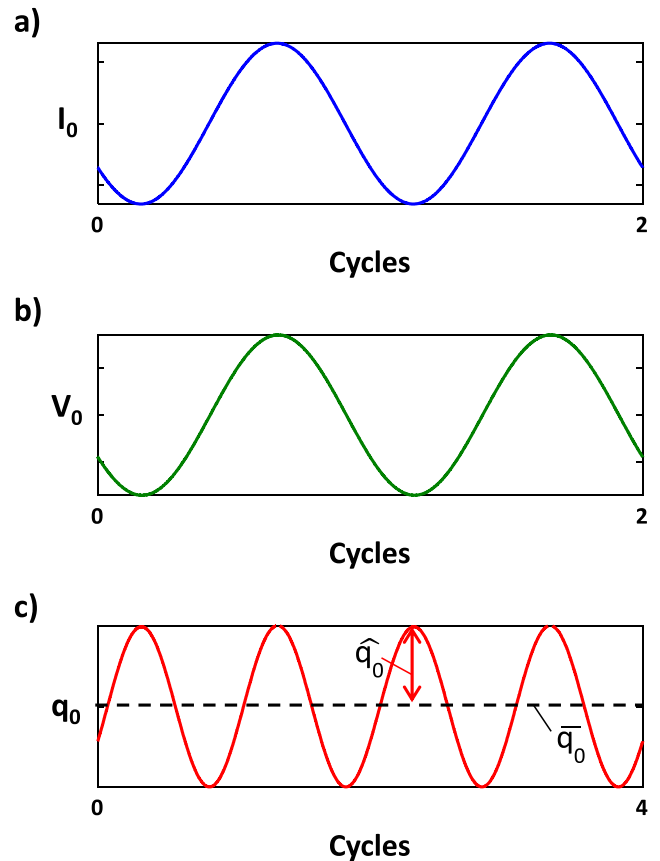

Figure 7. Example traces of (a) set cyclic variation in heater current; (b) measured voltage drop across the heater; and (c) calculated surface heat flux across four heating cycles (two current/voltage cycles).

current supply capable of modulating the current at frequencies from 0 to 50 kHz within 0.05% uncertainty of the current amplitude. This excitation current is represented in figure 7(a) over the course of two cycles. The current through the surface heater creates voltage modulations at the same frequency as
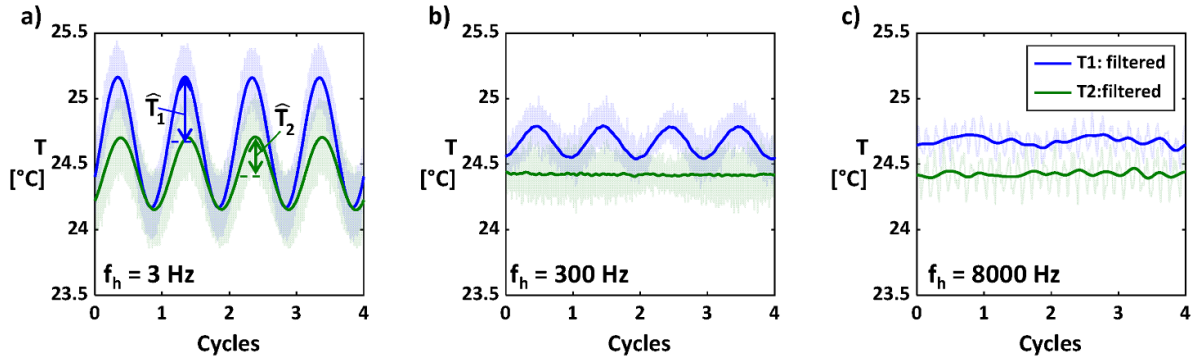
Figure 8. Temperature traces from the subsurface RTDs in response to cyclic surface heating at (a) 3 Hz, (b) 300 Hz, and (c) 8000 Hz.

illustrated in figure 7(b). The heat flux dissipated on the surface (q_0) can then be calculated though equation (7):

$$q_0 = \frac{V_0 I_0}{A_c} \tag{7}$$

where I_0 is the set current, V_0 is the voltage drop across the heater that is in-phase to the current, and A_c is the cross-section area of the heater. As shown in figure 7(c), this creates a heat flux at twice the frequency of the current and the voltage. The corresponding heating frequency (f_h) will be used throughout the remainder of this study to quantify the response of the device across different spectral ranges. Figure 7 serves as an example of one such f_h value.

Figure 7(c) illustrates that the surface heat flux (q_0) has a mean and fluctuating component. Importantly, the mean component through the device is not always equal to the fluctuating component. In a 1D analysis, the mean component will encounter an entire resistive network based upon the convection above the device and all the lower layers. However, the fluctuating component will be constrained to the resistance within the thermal penetration depth of the frequency. For that reason, the fluctuating components are much less sensitive to convection and radiation effects [21, 22]. Therefore, the fluctuating components will be used to determine the thermal properties.

To determine the thermal properties, both the boundary condition (q_0) and the temperature measurements (T_1 and T_2) are necessary. The previously described surface heating was damped through the coating and substrate layers causing attenuated temperature readings from the subsurface RTD measurements. Figure 8 displays the T_1 and T_2 measurements at different frequencies for the same heating power over four heating cycles (representative of figure 7(c)). The signals in figure 8 were acquired at 500 kHz for 3 s. Displayed in figure 8 is the filtered signal with the raw (translucent silhouette) signal behind it. The signal was filtered following the solution framework outlined by Siroka *et al* [12] using a zero-phase moving average filter constructed for a given heating frequency.

Figure 8 confirms several characteristics analytically predicted by figure 2. As the frequency increases, both $\widehat{T}_1$ and $\widehat{T}_2$ diminish. At the intermediate frequency of $f_h = 300$ Hz (figure 8(b)), $\widehat{T}_2$ is damped to a nearly DC output while $\widehat{T}_1$ still shows a distinct frequency response. At the design intent

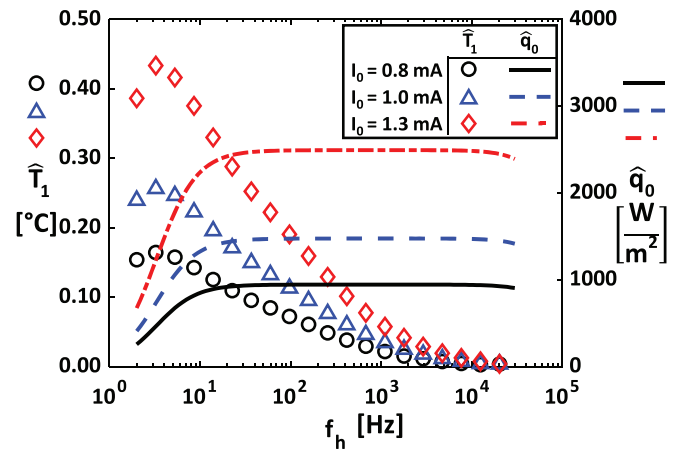**Figure 9.** T_1 and q_0 amplitude across a variety of heating frequencies for three discrete heating currents.

value, $f_h = 8000$, both the $\widehat{T}_1$ and $\widehat{T}_2$ signal appear to be within the noise in the instantaneous view. This may seem contradictory to figure 3, but stems from lower heating values than the design intent, which were limited by the allowable current through the surface heater.

To significantly reduce the noise floor of the experimental system and more accurately obtain the frequency cutoff and material properties, a lock-in amplifier was utilized. Lock-in amplifiers are ideal devices for detecting signals at prescribed frequencies in noisy environments [23]. For this experimental setup, the in-phase and out-of-phase voltage signals were measured with respect to the supplied current, which was used as a reference signal. Signal resolution was increased 100x through the lock-in amplifier when compared to conventional amplification. The left ordinate in figure 9 shows $\widehat{T}_1$ (plotted in symbols), while the right ordinate displays $\widehat{q_0}$ (plotted in lines). The logarithmic abscissa represents the heating frequency. For this experiment, the heating frequency was swept between 2 and 30 000 Hz at 100 logarithmically spaced points. Every fifth point is plotted in figure 9 for ease of interpretation.

Three discrete current values, I_0, were chosen to create varying levels of heating fluctuations, as identified in figure 9. These three I_0 values were on the same magnitude as the excitation current for the RTDs (1.0 mA for both I_1 and I_2).
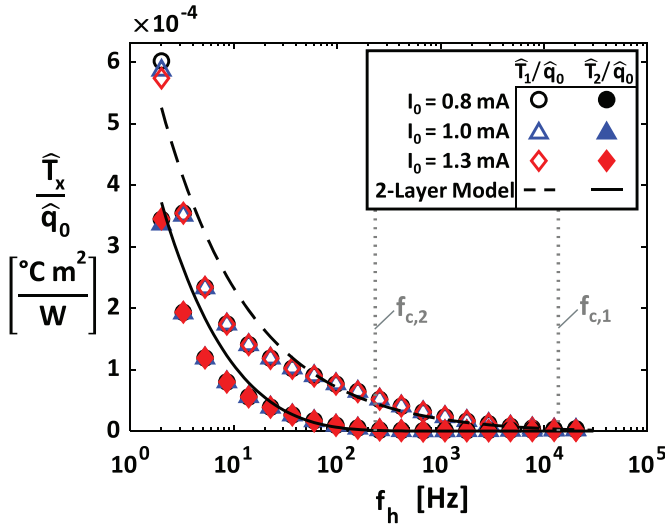
Figure 10. $\widehat{T}_1/\widehat{q}_0$ and $\widehat{T}_2/\widehat{q}_0$ across a range of heating frequencies with a 2-layer model plotted based on determined thermal properties. The maximum frequency response of each individual RTD is characterized by dashed lines.

However, the heater resistance was much greater than the RTDs, making the heat flux through the heater much higher than the RTDs. To ensure the excitation currents has a negligible effect on the results, this procedure was repeated with an order of magnitude lower excitation RTD current. Although not shown here for brevity, figure 9 was reproduced using the lower excitation current and no notable differences were seen in the measured temperatures, building confidence that the RTD current was sufficiently small compared to the supplied heat flux from the surface heater.

Figure 9 generally follows anticipated trends—in particular, the temperature rise is increased at high heat fluxes. Figure 9 also builds a better understanding of the frequency response of this device. For frequencies up to approximately 15 kHz, there is a measurable difference in the $\widehat{T}_1$ values between the different heating levels. This finding builds confidence that the frequency response is indeed within the design intent. Furthermore, at low frequencies, the measured heat dissipated through the heater was significantly lower than at higher heating frequencies due to capacitance effects in the heater. To account for these effects, only the in-phase voltage component to the current was used to calculate the heat flux.

Although the absolute value of the measured $\widehat{T}_1$ depends upon $\widehat{q}_0$, the thermal properties of the gauge should be independent of the selected heating values. Therefore, it is possible to collapse the curves in figure 9 by normalizing the temperature amplitude by the heat flux amplitude. Figure 10 illustrates the data presented in figure 9 though this form as open symbols, and the same relationship is added showing $\widehat{T}_2/\widehat{q}_0$ with filled symbols. Comparing the two measurement locations in figure 10, the lower amplitude of the T_2 measurement plane highlights the expected damping effect relative to the T_1 measurement plane. To quantify this effect, figure 10 identifies the respective cutoff frequency (defined as 0.05% of the initial

Table 2. Comparison of design thermal properties to measured values.

Parameter	Design	Measured	Difference
$(\rho_s c_s k_s)^{0.5}$	501	532	5.6%
k_s/d_s	3800	3842	1.1%
$(\rho_c c_c k_c)^{0.5}$	407	441	7.7%
k_c	0.12	0.117	2.6%
d_c	1E-6	1E-6	0%

value) for the T_1 and T_2 plane. Following this convention, the cutoff frequency for T_2 ($f_{c,2}$) was determined to be 233 Hz, while the cutoff frequency for T_1 ($f_{c,1}$) was determined to be 13 800 Hz.

As previously addressed, thermal properties are necessary to accurately convert the measured temperature to the surface heat flux. The thermal properties of this device were obtained following an iterative approach. Impulse response filters for the coated gauge [12, 24] were constructed using the nominal design parameters in table 1 as inputs including k_c, $(\rho_c c_c k_c)^{0.5}$, k_s/d_s, and $(\rho_s c_s k_s)^{0.5}$. These filters utilize inverse methods to transform the measured temperature to surface heat flux and rely on accurate thermal properties of the coating and substrate. The created filters were used with the data in figure 10 across the entire frequency range and the root-mean-square errors were calculated. A Nelder-Mead Simplex Method minimization scheme [25] was employed to perturb the thermal property filter inputs and minimize the root-mean-square errors between the input heat flux and the calculated heat flux. Table 2 displays the thermal properties deduced from this process and compares them to the nominal design values. The values in table 2 were between 2.6% and 7.7% different from the design values in table 1 with the exception of d_c which was measured with a profilometer and therefore held as a constant input. Note, these values represent the room temperature thermal and geometric properties. Heat flux errors can arise if the thermal and geometric property determination temperature is different from operating temperature of the HFG [11]. Therefore, it is imperative to accurately determine the thermal properties at the operating temperature of the HFG.

Determining the thermal parameters across an entire frequency range helps to ensure proper sensitivity to appropriate parameters. For example, at low frequencies, the impulse filters are more sensitive to direct mode heat transfer parameters such as k_s/d_s. On the other hand, coating properties and the thermal effusivity of the substrate become increasingly important at high frequencies [12]. As shown in figure 10, these parameters can then be used with the simplified 2-layer model to design devices according to desired specifications.

Comparing the measured data (symbols) and the analytical model (lines) in figure 10, the identified discrepancy at low frequencies is attributed to the fact that the model only accounts for two-layers where the second layer is a semi-infinite substrate. In the experimental setup, this assumption is only valid at high frequencies since at low heating frequencies the thermal wave will propagate into adhesion/

mounting layers below the HFG, affecting the temperature traces. However, the simplified model accurately captures the shape of the curve and becomes more accurate with increasing frequencies, making it a useful design tool for the first-order prediction of the frequency response and coating thickness determination.

4. Experimental verification

This section verifies that the material properties determined through the use of a lock-in amplifier and presented in the previous section will work with traditional amplification in the presence of signal noise, which can typically introduce processing challenges. First, the linearity of the mean heat flux will be verified. Then, the time-resolved heat flux deduction capacities will be quantified for two test cases.

4.1. Mean heat flux verification

Based upon equation (2), the mean heat flux, $\overline{q_0}$ should be a linear function of the change in temperature between the RTDs with a slope equal to k_s/d_s. This relationship is illustrated in figure 11, which plots $\overline{q_0}$ against ΔT across the HFG RTDs for a set of chosen frequencies. Figure 11 also displays the linear line with a $k_s/d_s = 3842$ ($\mathrm{Wm^{-2}\,K^{-1}}$), as determined in the previous section. The values of $\overline{q_0}$ plotted on the ordinate represent the calculated heat flux based upon equation (7) with corrections for mean heat flux lost to the surrounding environment. The uncertainty bounds plotted in figure 11 account for the uncertainty of the temperature calibrations, heater currents, and voltage acquisition, leading to an estimated overall uncertainty of 8% for mean heat flux. Through this approach, the linearity shown in figure 10 builds confidence in the ability to accurately measure mean heat flux independent of frequency. This relationship relates to the temperature traces illustrated in figure 8 through the insensitivity of the mean temperature difference across a range of frequencies.

4.2. Fluctuating heat flux verification

To verify the thermal properties important to the fluctuating heat flux in the previous section, the filtered temperature traces in figures 8(a) and (b) were processed using impulse response filters and are shown in figures 12(a) and (b) respectively. In figure 12, the values calculated using an impulse response approach are shown as solid lines with the measured q_0 values as dashed lines. Note that at 3 Hz, the component of the voltage in phase with the current was smaller than at 300 Hz as evidenced in figure 9, explaining the lower amplitude. These two cases are representative of the two operating regions of the HFG. At 3 Hz, both the T_1 and T_2 are critical to reconstruct the surface heating. At 300 Hz, only the T_1 trace is necessary for the fluctuating component, however, T_2 is still needed to quantify the mean value.

Based on the two test cases in figure 12, the relative amplitude difference between the calculated impulse response value and the measured heat flux is approximately 30% at $f_h = 3$ Hz and 10% at $f_h = 300$. This identified discrepancy at
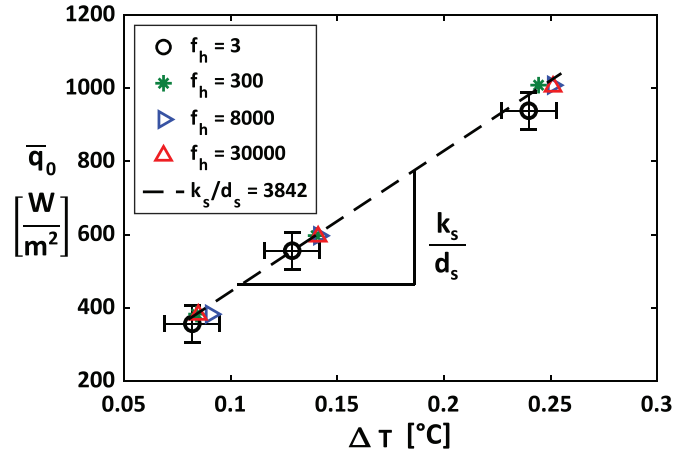

Figure 11. Measured mean heat flux plotted against the measured temperature difference for different heat frequencies under normal amplification.

the lower heating frequency is likely due to the uncertainty in measured heat flux when a large phase lag between the voltage and current is present. Further investigation is warranted to fully understand this issue.

5. Durability improvements

Until this point, the present study has detailed the design, fabrication, and complex processing necessary to account for the coating in high-frequency heat flux measurements. However, the primary function of the proposed coating is to add durability to the sensors. To test the durability of the chosen parylene-F coating compared to its uncoated counterpart, both types of sensors were installed in the START facility at Penn State University upstream of the test section. The sensors were adhered to a 0.5″ diameter probe along with a reference thermocouple (TC). Every uncoated sensor failed during the probe fabrication process, showcasing the poor durability from the outset. However, all of the coated gauges subject to the same processes at the same time remained functional. This initial qualitative outcome builds confidence in the robustness of the gauges.

After installation, six coated sensors were monitored over four consecutive days of a turbine test program to quantify the linearity of the sensors with respect to the TC. Figure 13 illustrates the voltage of a single RTD against the change in temperature of the nearby TC. A photo of the probe can be found in the bottom right of the plot. Because figure 13 represents a durability test, there was no specified heat flux through the part. Therefore, only V_1 (a proxy for T_1) values were obtained.

The different markers within figure 13 correspond to different days of testing. The agreement of the voltage measurements over this period illustrates the repeatability of the coated sensor design over repetitive test days and conditions. If calibration drift or resistance (voltage) changes due to surface erosion or oxidation were present over the course of the test, the linearity of the curve would have changed in the course of testing. However, a linear fit of the data in figure 13 results in
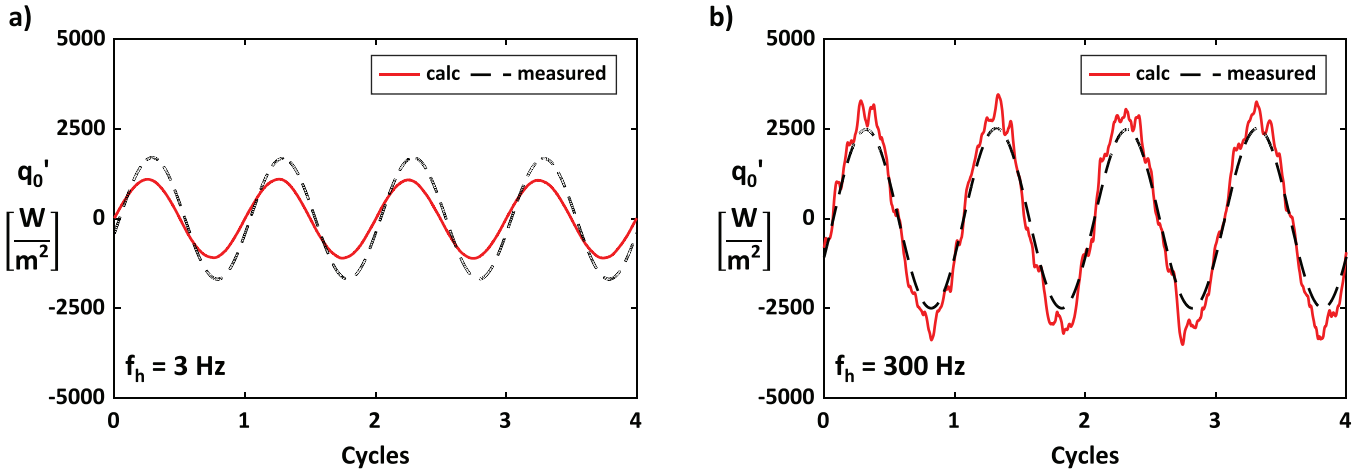
a)

b)

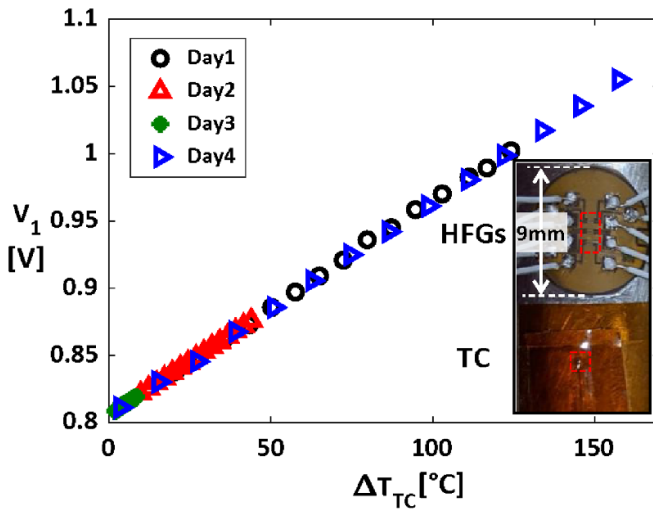Figure 12. Instantaneous q_0 over four surface heating cycles at (a) 3 Hz and (b) 300 Hz.

Figure 13. Voltage output of a single RTD (shown on the bottom right of the plot) with respect to a change in thermocouple temperature from the baseline condition.

an R^2 value of 0.998 while the mean deviation between the fit and the experimental data is 0.15 °C across all test days. This result confirms that coating is providing the necessary protection from the experimental environment.

To add perspective, figure 13 showcases that this sensor was functioning through 18 h of operation in a heated open loop facility just downstream of a combustion chamber with the remainder of the time representing cooldown periods between days (the facility does not operate 24 h a day). These 18 h of testing equate to roughly 20 years of testing runs in a short-duration facility [11]. Importantly, these devices were still functional upon removal.

6. Conclusions

Sensor survivability is one of the most important parameters for successful instrumentation deployment; the design, calibration, and processing schemes are irrelevant if the sensor is inoperable at installation. To that end, this study details the development of advanced HFGs capable of robust high-frequency measurements. First, using analytical solutions to the unsteady conduction equation, this work outlines the governing nondimensional parameters critical to the design of coated heat transfer gauges. Specifically, the nondimensional coating thickness (d_c/λ_c) was shown to be important to the attenuation of subsurface temperature signals. Given a set of end user heat transfer specifications, these processes were implemented in a practical manner to design a coated sensor applicable to turbine research facilities.

The sensors were manufactured using nanofabrication processes at Penn State University. The additional processing steps required to create a coated gauge were found to have no effect on device yield. Furthermore, a subset of the coated gauges were fabricated with an added surface heater to characterize the frequency response and thermal properties of the build. By modulating and measuring the surface heat flux at known frequencies, the frequency response of a coated HFG was characterized to be 13.8 kHz.

The thermal properties of the gauge were obtained through iterations of impulse response filters minimizing the root-mean-square error between the input heat flux and the heat flux calculated based upon the temperature signals. The gauge design and characterization outlined herein represents a unique approach for validating sensor design. Although there is an increased fabrication complexity from the addition of a surface heater, calibrating and verifying in this manner provides a complete system check that accounts for the calibration of the RTDs as well as the thermal properties of the system. Using the impulse response filters with correct thermal properties, the mean and time-varying heat flux error was quantified with respect to the measured surface heat flux. Mean heat flux errors of 8% and fluctuating heat flux errors of 10%–30% were noted.

The current work showcases the successful implementation and durability enhancement from the addition of a coating in a turbine test facility. Initial results show promising durability improvements for experimental testbeds of this type. This study has also addressed

several challenges with the design and implementation of coated sensors. Ultimately, methods presented throughout this document can be extended to a variety of applications in the thermal-fluidic sciences and serves as a guide for the design and validation of coated thermal sensors.

Data availability statement

The data that support the findings of this study are available upon reasonable request from the authors.

Acknowledgments

Disclaimer

ORCID iDs

Shawn Siroka https://orcid.org/0000-0001-9405-3004
Reid A Berdanier https://orcid.org/0000-0001-9204-4710

References

[1] Carter T J 2005 Common failures in gas turbine blades *Eng. Fail. Anal.* **12** 237–47

[2] Sieverding C H, Arts T, Dénos R and Brouckaert J F 2000 Measurement techniques for unsteady flows in turbomachines *Exp. Fluids* **28** 285–321

[3] Wright L M and Han J-C 2013 Heat transfer enhancement for turbine blade internal cooling *J. Enhanced Heat Transfer* **55** 321–52

[4] Spakovszky Z S Instabilities everywhere! Hard problems in aero-engines GT2021–60864

[5] Childs P R N, Greenwood J R and Long C A 1999 Heat flux measurement techniques *Proc. Inst. Mech. Eng.* C **213** 655–77

[6] Epstein A H, Guenette G R and Norton R J G 1985 The design of the MIT blowdown turbine facility GTL Report 183 (available at: https://dspace.mit.edu/bitstream/handle/1721.1/104724/16206191.pdf?sequence=1)

[7] Anthony R J, Clark J P, Kennedy S W, Finnegan J M, Johnson D, Hendershot J and Downs J Flexible non-intrusive heat flux instrumentation on the AFRL research turbine GT2011–46853

[8] Nickol J B and Mathison R M 2015 Time-resolved heat transfer and surface pressure measurements for a fully cooled transonic turbine stage *J. Turbomach.* **137** 091009-1–10

[9] Chana K, Cardwell D and Jones T 2013 A review of the oxford turbine research facility GT2013–95687

[10] Epstein A H, Guenette G R, Norton R J G and Yuzhang C 1986 High-frequency response heat-flux gauge *Rev. Sci. Instrum.* **57** 639–49

[11] Siroka S, Berdanier R A, Thole K A, Chana K, Haldeman C W and Anthony R J 2020 Comparison of thin film heat flux gauge technologies emphasizing continuous-duration operation *J. Turbomach.* **142** 091001-1–10

[12] Siroka S, Berdanier R A and Thole K A 2021 Two-layer transient heat transfer using impulse response methods *Int. J. Heat Mass Transfer* **170** accepted

[13] Barringer M, Coward A, Clark K, Thole K A, Schmitz J, Wagner J, Alvin M A, Burke P and Dennis R The design of a steady aero thermal research turbine (START) for studying secondary flow leakages and airfoil heat transfer GT2014–25570

[14] Siroka S, Monge-concepción I, Berdanier R A, Barringer M D, Thole K A and Robak C W Correlating cavity sealing effectiveness to time-resolved rim seal events in the presence of vane trailing edge flow GT2021–59285

[15] VSI Parylene 2020 The complete guide to parylene coatings *Technical Data Sheet*

[16] Celestina R, Sperling S, Christensen L, Mathison R, Aksoy H and Liu J Development of new single and high-density heat-flux gauges for unsteady heat transfer measurements for a rotating transonic turbine GT2020–14527

[17] Anthony R J, Jones T V and LaGraff J E 2005 High frequency surface heat flux imaging of bypass transition *J. Turbomach.* **127** 241–50

[18] Collins M, Chana K and Povey T 2015 New technique for the fabrication of miniature thin film heat flux gauges *Meas. Sci. Technol.* **26** 025303-1–9

[19] Siroka S, Foley B M, Berdanier R A and Thole K A 2021 Application of 3-omega method for thin-film heat flux gauge calibration *Meas. Sci. Technol.* **32** 114001

[20] Zilles D 1999 The effect of non-isothermal wall boundary temperature on convective heat flux over a flat plate *Master's Thesis* The Ohio State University

[21] Dames C 2013 Measuring the thermal conductivity of thin films: 3 omega and related electrothermal methods *Annu. Rev. Heat Transfer* **16** 7–49

[22] Cahill D G 1990 Thermal conductivity measurement from 30 to 750 K: the 3ω method *Rev. Sci. Instrum.* **61** 802–8

[23] Scofield J H 1994 Frequency-domain description of a lock-in amplifier *Am. J. Phys.* **62** 129–33

[24] Oldfield M L G 2008 Impulse response processing of transient heat transfer gauge signals *J. Turbomach.* **130** 021023-1–9

[25] MathWorks Fminsearch (available at: www.mathworks.com/help/matlab/ref/fminsearch.html) (Accessed 08 October 2021)